Surface & Coatings Technology 206 (2011) 1765–1770

Contents lists available at ScienceDirect

Surface & Coatings Technology

journal homepage: www.elsevier.com/locate/surfcoat

Modeling reactive sputter deposition of titanium nitride in a triode magnetron sputtering system

J.C. Sagás [a,*], D.A. Duarte [a], D.R. Irala [a,b], L.C. Fontana [b], T.R. Rosa [a]

[a] Technological Institute of Aeronautics, Plasmas & Processes Laboratory, 12228-900, S. J. dos Campos, Brazil
[b] Santa Catarina State University, Plasma Physics Laboratory, 89223-100, Joinville, Brazil

ARTICLE INFO

Available online 18 July 2011

Keywords:
Berg's model
Magnetron sputtering
Titanium nitride

ABSTRACT

In this paper, the so-called Berg's model was successfully employed in order to model the reactive sputter deposition of titanium nitride (TiN) by a triode magnetron sputtering (TMS) system. Such system consists of a grounded grid introduced between the target and the substrate. The grid acts as the anode, and the glow discharge is formed between the target and grid. The qualitative model was compared to experimental data. In addition, results from a conventional MS system were also compared to the ones from the modified TMS system. It was possible to observe that (a) the width of the hysteresis region is narrower for TMS for all modeled conditions; (b) the hysteresis width increases as a function of grid-to-target distance.

1. Introduction

Reactive magnetron sputtering deposition is a well known technique for thin film deposition, and it has a wide range of applications [1–3]. Despite the advantages of this method regarding the control of film properties and structure [4], reactive deposition has some drawbacks related to the phenomenon of target poisoning. When the reactive gas is added to the chamber, it reacts not only on film surface but also on metal target surface. The compound formation on the metal target reduces significantly the deposition rate, and the addition of the reactive gas to the process causes the hysteresis effect. Initially, the added gas is consumed due to the reactions with the target and with the metal deposited on the chamber walls and substrate surface. Therefore, the partial pressure of the reactive gas remains at a very low level until the surfaces become almost completely covered by the compound, which leads to an abrupt reduction in gas consumption, and, consequently, in an abrupt increase in pressure. After this, reducing the reactive gas flow rate leads first to a small decrease in partial pressure, and second to an abrupt drop in pressure. This behavior results in a hysteresis loop which can be observed through a graph showing the reactive gas partial pressure as a function of the total reactive gas flow rate. The hysteresis loop leads to instabilities when the process is controlled by the reactive gas flow [5].

To avoid these problems, it is important to understand all the phenomena that occur during reactive sputter deposition. To do this, it is essential to formulate a reliable model for reactive (magnetron) sputtering. Berg et al. proposed a qualitative model to describe the reactive sputter deposition at a steady-state [5–7], this model can be reliably used to describe the general features of the process, that is, the hysteresis loop and how the deposition parameters (geometrical, physical or chemical) affect the width of the hysteresis region.

Berg's model assumes that the target current is constant, and it also hypothesizes that the reactions between gas molecules and surfaces only occur by chemisorption. Although more recent papers [8,9] have shown that the ion implantation plays an important role in reactive sputtering, chemisorption seems to be the predominant reactive mechanism, especially when the reactive gas and the metal present a high chemical reactivity [10].

Berg's model is based on the balance equations for compound formation at a steady state on the target area (A_t) and collecting area (A_c), where the latter includes the substrate and chamber walls. When the reactive gas is added, a molecular flux F towards all surfaces occurs according to Eq. (1):

$$F = \frac{p}{\sqrt{2\pi mkT}} \tag{1}$$

where p is the reactive gas pressure, m the mass of the reactive gas molecule, k the Boltzmann constant and T the gas temperature.

On the target surface, compound formation occurs due to reactions between gas and metal, while compound removal occurs due to sputtering. Thus, the balance equation on the target can be written as:

$$\frac{J}{q} Y_c \theta_t = 2\alpha F(1-\theta_t) \tag{2}$$

where J is the ion current density, q is the ion charge, Y_c is the compound sputtering yield, α is the sticking coefficient and θ_t is the

* Corresponding author. Tel.: +55 12 3947 5942.
E-mail address: juliocesarsagas@gmail.com (J.C. Sagás).

0257-8972/$ – see front matter © 2011 Elsevier B.V. All rights reserved.
doi:10.1016/j.surfcoat.2011.07.013

fraction of the target area covered by compound. The number of sputtered particles per second of metal and compound is given by

$$F_c = \frac{J}{q} Y_c \theta_t A_t \tag{3}$$

$$F_m = \frac{J}{q} Y_m (1-\theta_t) A_t \tag{4}$$

where F_c and F_m are the compound and metal flow rates, respectively, and the total sputtering erosion rate is given by the sum of F_c and F_m. Y_m is the sputtering yield of the metal. On collecting area, the compound formation balance is due to reactions with the reactive gas and to the compound and metal deposition sputtered from the target. Thus, the collecting area balance equation is:

$$2Q_c + F_c(1-\theta_c) = F_m \theta_c \tag{5}$$

where θ_c is the fraction of the collecting area covered by compound and Q_c is the reactive gas consumed on the collecting area. The factor "2" is valid only for diatomic gasses that lead to the formation of two compound molecules (*e.g.*, $2Ti + N_2 \rightarrow 2TiN$). The gas consumed on the collecting and target surfaces, respectively, are described by the following equations:

$$Q_c = \alpha F (1-\theta_c) A_c \tag{6}$$

$$Q_t = \alpha F (1-\theta_t) A_t \tag{7}$$

and the total gas flow rate is:

$$Q_{total} = Q_t + Q_c + Q_p \tag{8}$$

where Q_p is the remaining part of the reactive gas that escapes from the processing chamber through the pumping system. Now, with this set of equations it is possible to model the reactive sputter deposition. For a detailed description see Ref. [5].

It is important to keep in mind that Berg's model is a first order approximation; still, it can adequately describe the general features of the reactive sputter deposition. The Berg's model has been improved: these improvements include effects such as ion implantation [10], the variation of the sticking coefficient [11], the variation of the secondary electron yield [12], the role of the sputtering yield [5,13], a non-uniform distribution of the current on the target surface [14], plasma chemistry [15,16], co-sputtering processes [17] and the deposition with two reactive gasses [18]. From other related papers, based on the Berg's model and experimental results, it is possible to observe that the hysteresis loop can be decreased, and sometimes extinguished through (1) increasing the pumping speed, (2) decreasing the target area and/or the collecting area [5], (3) using reactive gas pulsing [19], (4) the HiPIMS technique [20], and (5) the "baffled target" reactive sputtering [21].

Fontana and Muzart developed another approach to the "hysteresis problem". That is, they proposed the so-called triode magnetron sputtering (TMS) system [22,23]. According to this configuration, a grid is inserted between the target and the substrate. When the grid is kept grounded, it becomes the discharge anode. A variation in the grid-to-target distance (d_{g-t}) modifies the plasma volume and conductivity. This system has been used in film deposition of different compounds [24–26]. It is noteworthy that regarding the TMS, the most interesting phenomenon, is the hysteresis control for the reactive deposition of TiN films [23]. Another important characteristic of this system is that the plasma is more stable than the one of the traditional magnetron sputtering [22,23]. However, the hysteresis control mechanisms of a TMS system have not been well explained yet. Thus, in order to investigate this TMS characteristic, the present work has adapted Berg's model to the TMS system. More specifically, Berg's model has been modified so as to model the reactive sputter deposition of TiN by the TMS system. The theoretical framework was qualitatively compared and correlated to experimental data.

2. Berg's model applied to the triode magnetron sputtering (TMS) system

The flow of sputtered material from the target in a triode magnetron sputtering system is schematically shown in Fig. 1. The insertion of the grid entails the existence of one extra surface next to the target. All processes that occur on the grid surface are similar to those ones occurring on the collecting area. The amount of TiN compound which is deposited on the grid is directly related to (1) the chemical reactions between the sputtered metal atoms and the reactive gas, and (2) the deposition of the compound (TiN) sputtered from the target. On the other hand, the decrease of the compound fraction on the grid surface is caused by deposition of metallic atoms. The grid position in the reactor (between the target and the substrate) will have an influence on the conditions of the collecting area. This effect is produced because part of the material sputtered from the target is collected on the grid, thus reducing the amount of material deposited on the collecting area.

Once sputtered, ejected target particles are randomly spread; therefore, the fraction of material deposited on the grid depends on the ratio between the grid area (A_g) and the transversal area of flow of the sputtered particles at this specific grid position (A_{st}), see Fig. 2. The effective grid area is the area where the deposition occurs. The amount of sputtered particles per time and per area units are F_c/A_{st} and F_m/A_{st} respectively for compound and metal. Consequently, $(F_c/A_{st})\ A_g$ expresses the fraction of the compound deposited on the grid and $(F_m/A_{st})\ A_g$ expresses the fraction of the metal deposited on the grid. The remaining sputtered material that has not been collected on the grid will be deposited on the collecting area. These remains are quantified as $F_c\ (1-A_g/A_{st})$ and $F_m\ (1-A_g/A_{st})$. Therefore, the ratio A_g/A_{st} has an important effect on the reactive sputter deposition in a TMS system.

Due to the uncertainties over the estimation of A_{st} in the present experiment, the ratio A_g/A_{st} is being presently employed as an input parameter, and we will refer to this ratio as β. For a fixed grid area, a

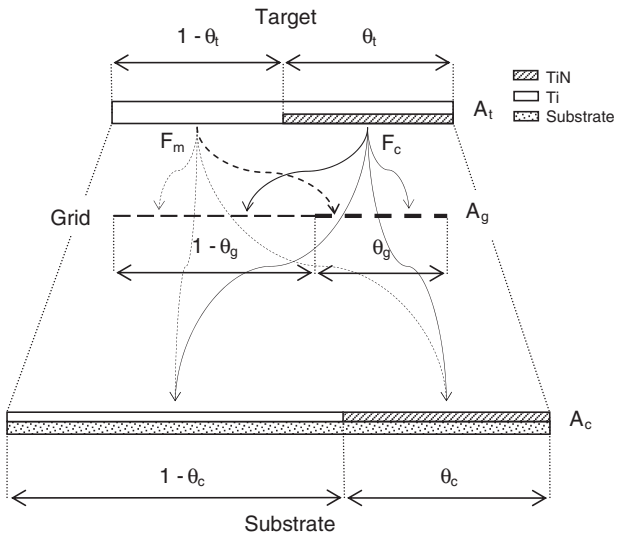

Fig. 1. Illustration of the sputtered material flows to the collecting (A_c) and grid (A_g) areas in a triode magnetron sputtering system.

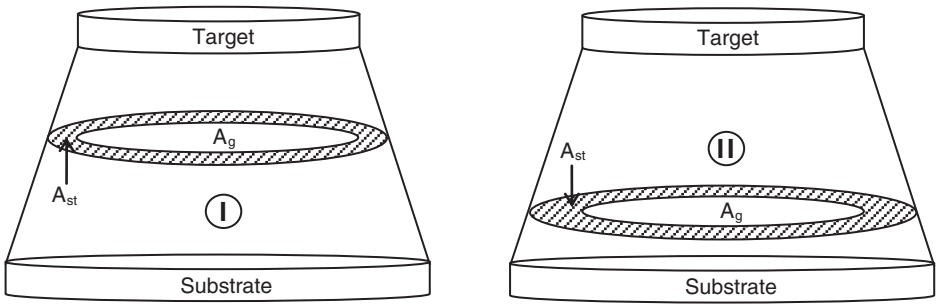

$$\beta = \frac{A_g}{A_{st}} \therefore \beta_I > \beta_{II}$$

Fig. 2. Influence of the grid-to-target distance in the value of β. In the case I, a low grid-to-target distance implies in a high β. In the case II, β decreases with increased grid-to-target distance due to the increase in the transversal area of the sputtered particles flow (A_{st}).

high value of β entails a grid closer to the target (smaller A_{st}). Thus, the balance equation for the compound on the grid is:

$$2Q_g + F_c\left(1-\theta_g\right)\beta = F_m\theta_g\beta \tag{9}$$

where Q_g is the gas consumed on the grid surface and θ_g is the fraction of the grid area covered by the compound. Then, the gas consumed on the grid can be written as:

$$Q_g = \alpha F\left(1-\theta_g\right)A_g \tag{10}$$

The flow rates of the compound and of the metal on the collection area are reduced by the factor $(1-\beta)$ because the grid is next to the target. So, the balance equation for the collecting area is

$$2Q_c + F_c(1-\theta_c)(1-\beta) = F_m\theta_c(1-\beta) \tag{11}$$

and the total reactive gas flow rate is now given by:

$$Q_{total} = Q_t + Q_c + Q_g + Q_p \tag{12}$$

Then, Eqs. (1) to (4) and (9) to (12) together with Eqs. (6) and (7) make it possible for us to model the reactive sputter deposition in a TMS system. For $A_g = 0$, the equations are made equal to the equations of the conventional magnetron sputtering system.

The equations just above are similar to the equations of the so-called "baffled target" reactive sputtering [21]. In the "baffled sputtering", the metal target is enclosed within a box which contains a window in front of the target erosion area. This system is employed so as to prevent the reactive gas from reaching the target. As a result, there is a difference in reactive gas pressure between the box and the main chamber. Similarly to the TMS system, part of the sputtered material is "trapped" so that it cannot reach the collecting area. However, the TMS does not employ the grid to enclose the target; the grid is used as an obstacle between the target and the substrate. Thus, in the model for the TMS system, there is not a difference in pressure between the area surrounding the target and the rest of the chamber.

3. Experimental setup

Experimental hysteresis curves were obtained through a Ti target (99.9%) sputtering in an atmosphere of Ar (99.99%) and N_2 (99.99%). The experiments were carried out in a stainless steel chamber ($\Phi = 30$ cm and $h = 25$ cm, see Fig. 1). Before the experiments, the chamber was evacuated to a background pressure of approximately 1.3 mPa. The rectangular target had dimensions of 132×100 mm with an erosion zone of 70 cm^2. In the experiments, no substrate or substrate holder was used. The gas pressure inside the chamber was monitored by capacitive (Baratron) and Penning gages. The argon pressure was fixed at 0.4 Pa, and the flow rate was 5.4 sccm. The nitrogen flow rate varied from 0.0 to 3.0 sccm, which led to a maximum nitrogen partial pressure of 0.3 Pa, varying according to the grid-to-target distance. The grid was made of austenitic stainless steel, and it was kept grounded in all experiments. The grid-to-target distance varied between 15 and 30 mm. The maximum input power was 475 W. During the experiments, the discharge current was set up at 0.8 A.

4. Theoretical model input data

TiN reactive sputter deposition was modeled for both MS and TMS systems. The sticking coefficient for N on Ti was overestimated and set to a unity. A lower sticking coefficient reduces the hysteresis effect because the probability of compound formation decreases. However, as the objective of this work is to clarify the effect of the grid, this overestimation does not affect the qualitative comparisons. The sputtering yields for Ti (Y_m) and TiN (Y_c) were taken as 0.63 and 0.43, respectively, for Ar^+ at 500 eV [27]. At higher partial pressure of the reactive gas, both the ions N^+ and N_2^+ will contribute to the target sputtering. However, this is not taken into account in the present model. Neither is the discharge voltage variation as a function of gas composition being considered. The introduction of these effects in the model is expected to increase the accuracy of the results. We note that the present work keeps the model as simple as possible so as to focus on the grid effect. The pumping speed was adjusted to 25 $l.s^{-1}$

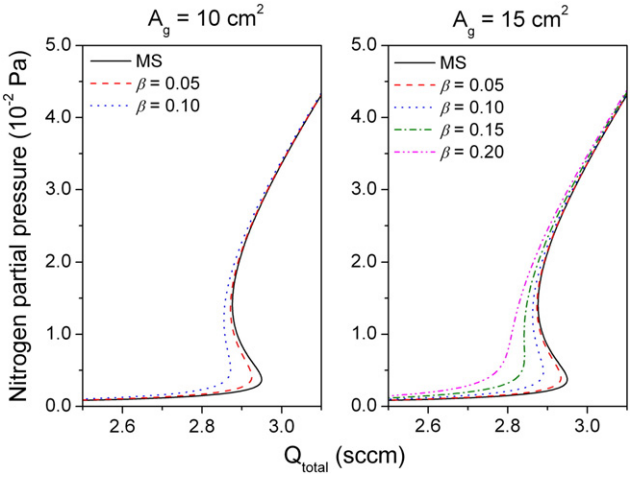

Fig. 3. The nitrogen partial pressure (p) as a function of the total nitrogen flow rate (Q_{total}) for MS and TMS systems.

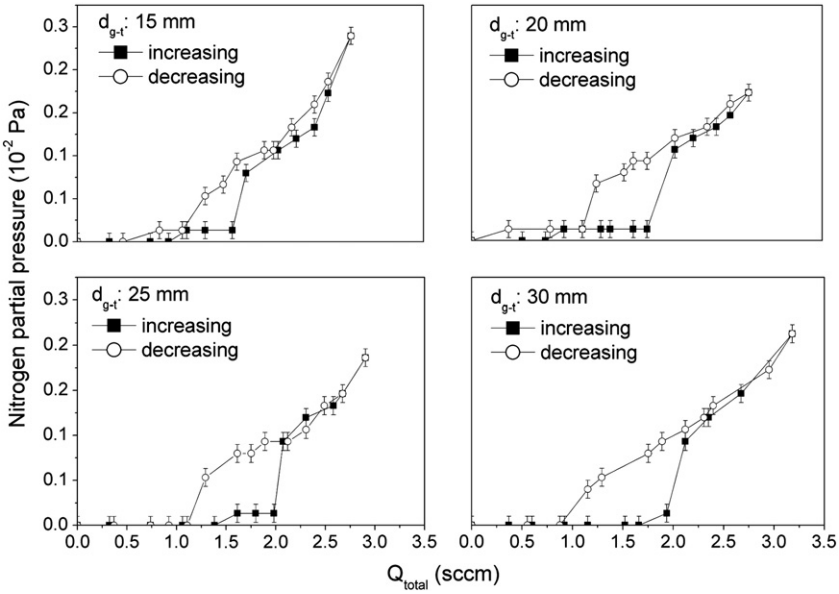

Fig. 4. Experimental data of the nitrogen partial pressure (p) as a function of the total nitrogen flow rate (Q_{total}) at different grid-to-target distances (d_{g-t}).

($0.025\ m^3.s^{-1}$) and the target and collecting areas were estimated as 70 cm^2 and 1580 cm^2, respectively. The target area was estimated as the target erosion zone. The collecting area was estimated through measuring the area where the deposition is visually perceptible without taking into account the non-uniform deposition on the chamber walls. The ion current on the target was set as 0.80 A. It can be pointed out that, during the experiments, oscillations on the discharge current were observed. For the TMS system, three grids with different areas were modeled, *i.e.* 10, 15 and 20 cm^2. Five different values of β were used to evaluate the effect of the grid-to-target distance (0.05, 0.10, 0.15, 0.20 and 0.25). The highest valid β value for each grid area is determined by the condition $A_{st}>A_t$.

5. Results and discussion

Comparing the modeling results for MS and TMS, it is possible to observe that the width of the hysteresis region is narrower for TMS for all modeled conditions, as shown in Fig. 3. The S-shaped behavior defines a hysteresis region where one value for Q_{total} may be satisfied by three different values of p, θ_t and θ_c [5]. It is noticed that by increasing β, the hysteresis width is reduced; in addition, for $\beta>0.15$, the hysteresis is not observed. From these figures, it can also be seen that by increasing β, the nitrogen partial pressure starts to increase faster as the nitrogen flow rate increases. The same behavior is identified from the experimental data, as shown in Figs. 4 and 5, where it is possible to see that the hysteresis width increases as a function of grid-to-target distance.

Fig. 5 shows the experimental data of the hysteresis width and maximum nitrogen flow rate before the nitrogen partial pressure starts to increase as a function of the grid-to-target distance. An increase of the grid-to-target distance is equivalent to a decrease of β. Although the quantitative comparison is not possible here, the model predictions were confirmed: it is observed a decrease of the hysteresis loop, and a faster increase of partial pressure with increased β (decreased grid-to-target distance).

The well defined S-shape curve can also be seen in the sputtering erosion rate as function of the total nitrogen flow rate, as shown in Fig. 6 for the grid area of 15 cm^2. From these curves, it is observed that the sputtering erosion rate decreases with increased β (decreased grid-to-target distance), that is, not only the deposition rate (the amount of material deposited on the collecting area), but also the number of particles sputtered from the target are reduced with

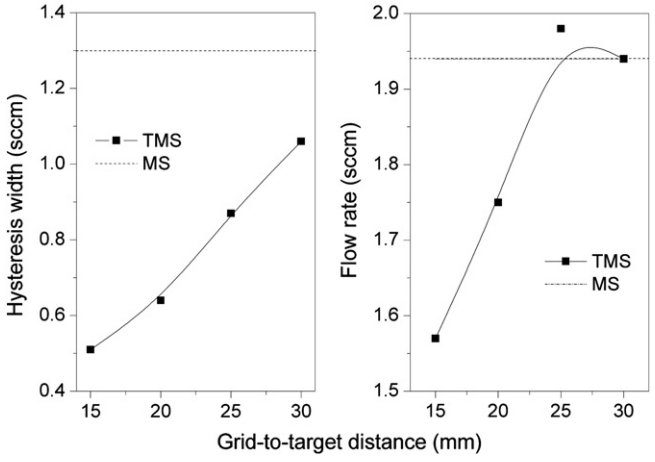

Fig. 5. Width of the hysteresis region (left) and maximum nitrogen flow rate before the nitrogen partial pressure starts to increase (right) as a function of the grid-to-target distance (d_{g-t}).

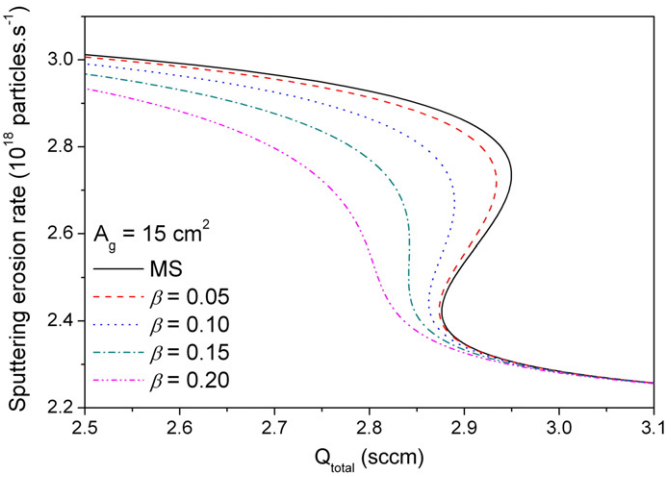

Fig. 6. The sputtering erosion rate as a function of the total nitrogen flow rate (Q_{total}) for MS and TMS systems.

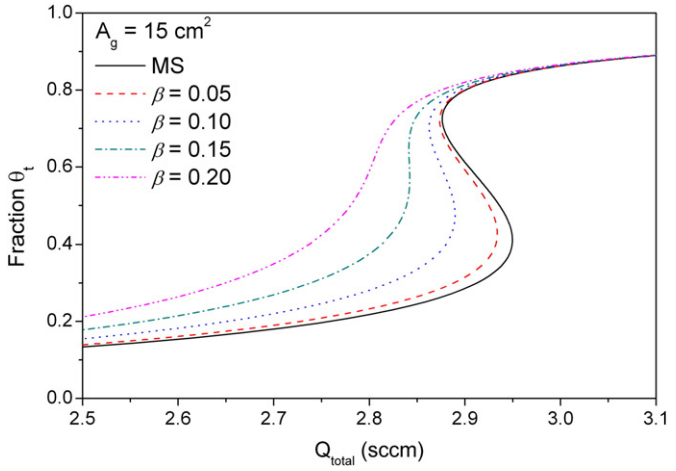

Fig. 7. The fraction of compound on the target surface (θ_t) as a function of the nitrogen flow rate (Q_{total}) for MS and TMS systems.

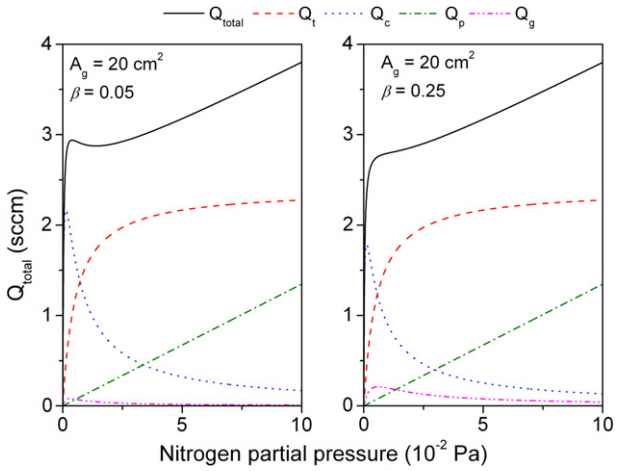

Fig. 9. The gas consumption by the target (Q_t), collecting area (Q_c), grid (Q_g) and pumping system (Q_p) as a function of the nitrogen partial pressure (p) for TMS system. The total nitrogen flow rate (Q_{total}) is the sum of the terms Q_t, Q_c, Q_p and Q_g, as can be seen in Eq. (12).

increased β. This reduction can be explained by taking into account the behavior of θ_t as a function of β. From Fig. 7, it can be observed that the target becomes poisoned faster as β increases. Then, as the sputtering yield of TiN is lower than that of Ti, the sputtering erosion rate decreases faster with increased β (Fig. 6).

To understand the reduction of the hysteresis loop, it is important to observe the behavior of the gas consumption on each surface. The hysteresis results from a negative derivative on the curve of the total reactive gas flow as a function of the partial pressure. This negative derivative is caused by the abrupt drop in gas consumption on the collecting area. This drop is caused by the almost complete coverage of the surface with the compound [5], as shown in Fig. 8 for a MS system.

As the grid is introduced, the reactive gas consumption is reduced on the collecting area due to the reduction of deposited material because part of the sputtered particles is "trapped" on the grid surface. Thus, when the grid is employed, gas consumption on the collecting area decreases as it can be seen in Fig. 9. At β higher than 0.15, the reduction of Q_c is so high that the contributions of Q_t, Q_g and Q_p prevent the hysteresis. Fig. 10 shows the behavior of the gas consumption on the collecting and grid areas as a function of the total nitrogen flow rate

It can be pointed out that at fixed β the hysteresis width region increases with increased grid area (Fig. 11). The reason for the greater hysteresis width at larger grid areas is as follows: the shape of the curve of the gas consumption on the grid is similar to that on the collecting area as the processes on each surface are identical. Thus, for a fixed β, a larger grid area entails a greater consumption of reactive gas by the grid (Fig. 12), which results in a larger hysteresis region. From this, it can be concluded that the principal effect of the grid regarding the reduction of the hysteresis loop is as follows: a decrease in gas consumption on the collecting area due to material deposition and gas consumption on the grid.

A specific detail of the TMS system was not taken into account in the present model, that is, the plasma is confined between the target (cathode) and the grid (anode), thus the chemical reactivity in this region (with plasma) is quite different from the reactivity around the collecting area (without plasma). In the region between the target and the grid, there is a great amount of nitrogen dissociation and nitrogen excitation. The region between the grid and the collecting area is a post-discharge region: the presence of radicals and reactive species is due only to the flow of these species from the space between the target and the grid. Thus, it can be expected that the gas consumption in the target-grid region (in the plasma volume) is greater than in the post-discharge zone. This effect can lead to a reduction in the reactive gas partial pressure between the target and the grid. This is an important modification that can be introduced to the model in the future.

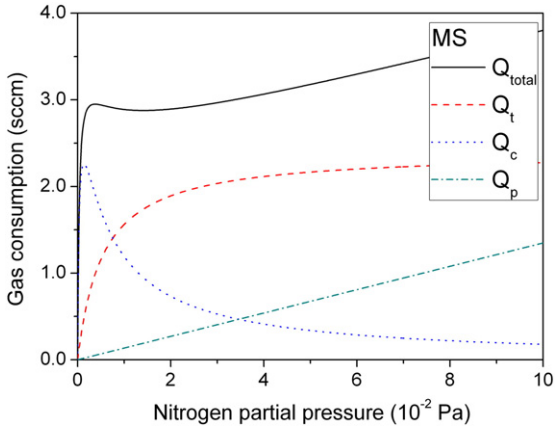

Fig. 8. The gas consumption by the target (Q_t), collecting area (Q_c) and pumping system (Q_p) as a function of the nitrogen partial pressure (p) for MS system. The total nitrogen flow rate (Q_{total}) is the sum of the terms Q_t, Q_c and Q_p, as can be seen in equation Eq. (8).

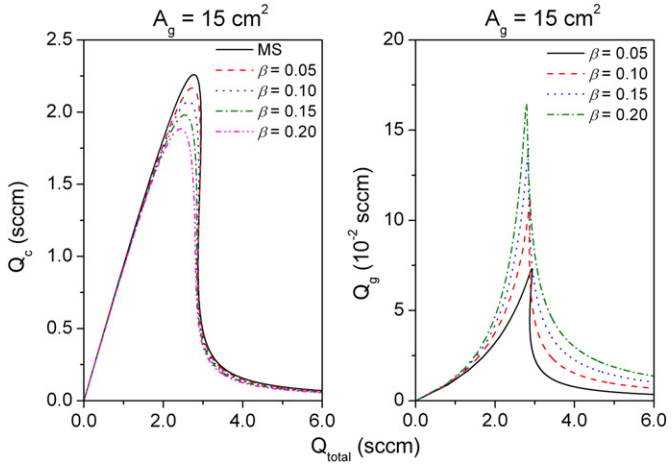

Fig. 10. The gas consumption on the collecting (Q_c – left) and grid areas (Q_g – right) at different values of β.

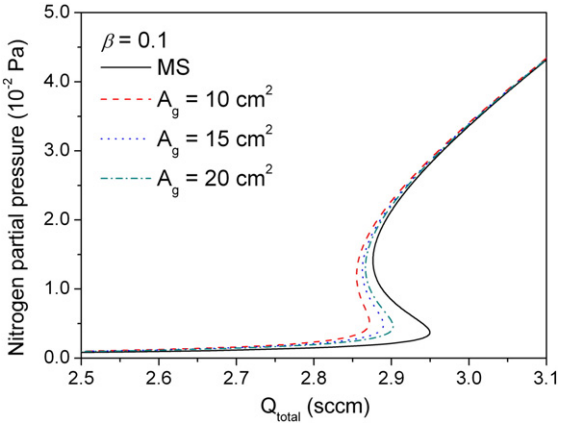

Fig. 11. The nitrogen partial pressure (p) as a function of the total nitrogen flow rate (Q_{total}) at different grid areas (A_g) for $\beta = 0.1$.

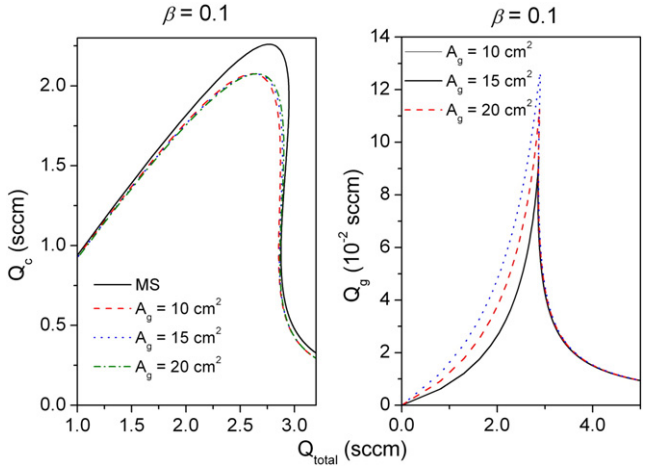

Fig. 12. The gas consumption on the collecting (Q_c – left) and grid areas (Q_g – right) at different grid areas (A_g) for $\beta = 0.1$.

6. Conclusions

The present paper has successfully employed Berg's model to a triode magnetron sputtering system. The main goal was to investigate the influence of the grid-to-target distance on the hysteresis loop. Results indicate that as the grid-to-target distance decreases, the hysteresis loop will also decrease. This reduction occurs because the introduction of the grid reduces gas consumption on the collecting area (A_c); as a result, the grid will "effectively" reduce A_c. Then, with a lower amount of compound and metal deposited on the collecting area, the gas consumption Q_c will decrease and Q_g will not compensate this reduction in Q_c. Thus, the nitrogen partial pressure will increase faster for lower nitrogen flow rates, reducing the hysteresis loop.

Acknowledgments

Authors would like to thank CAPES, FAPESP and the National Network for Cooperation in Plasma Engineering (RECONPLASMA) by their financial support.

References

[1] N. Hellgren, M.P. Johansson, E. Broitman, L. Hultman, J.E. Sundgren, Phys. Rev. B 59 (1999) 5162.
[2] V. Stranak, M. Quaas, R. Bogdanowicz, H. Steffen, H. Wulff, Z. Hubicka, M. Tichy, R.J. Hippler, Phys. D: Appl. Phys. 43 (2010) 285203.
[3] S. Mahieu, D. Depla, J. Phys. D: Appl. Phys. 42 (2009) 053002.
[4] S.E. Rodil, J.J. Olaya, J. Phys. Condens. Matter 18 (2006) S1703.
[5] S. Berg, T. Nyberg, Thin Solid Films 476 (2005) 215.
[6] S. Berg, H.-O. Blom, T. Larsson, C. Nender, J. Vac. Sci. Technol. A 5 (2) (1987) 202.
[7] S. Berg, H.-O. Blom, M. Moradi, C. Nender, T. Larsson, J. Vac. Sci. Technol. A 7 (3) (1989) 1225.
[8] D. Depla, G. Buyle, J. Haemers, R. De Gryse, Surf. Coat. Technol. 200 (2006) 4329.
[9] D. Depla, S. Mahieu, R. De Gryse, Thin Solid Films 517 (2009) 2825.
[10] D. Depla, S. Heirwegh, S. Mahieu, R. De Gryse, J. Phys. D: Appl. Phys. 40 (2007) 1957.
[11] Chuan Li, J.H. Hsieh, J. Phys. D: Appl. Phys. 37 (2004) 1065.
[12] Y. Matsuda, K. Otomo, H. Fujiyama, Thin Solid Films 390 (2001) 59.
[13] T. Kubart, T. Nyberg, A. Pflug, M. Siemers, M. Augsten, D. Koehl, M. Wuttig, S. Berg, Surf. Coat. Technol. 204 (2010) 3882.
[14] P. Vasina, T. Hytková, M. Eliás, Plasma Sources Sci. Technol. 18 (2009) 025011.
[15] A. Ershov, L. Pekker, Thin Solid Films 289 (1996) 140.
[16] Chuan Li, J.H. Hsieh, W.M. Huang, Surf. Coat. Technol. 198 (2005) 372.
[17] M. Moradi, C. Nender, S. Berg, H.-O. Blom, A. Belkind, Z.J. Orban, J. Vac. Sci. Technol. A 9 (3) (1991) 619.
[18] C. Rousselot, N. Martin, Surf. Coat. Technol. 142–4 (2001) 206.
[19] W.D. Sproul, Surf. Coat. Technol. 33 (1987) 73.
[20] E. Wallin, U. Helmersson, Thin Solid Films 516 (2008) 6398.
[21] F. Engelmark, J. Westlinder, T. Nyberg, S. Berg, J. Vac. Sci. Technol. A 21 (6) (2003) 1981.
[22] L.C. Fontana, J.R.L. Muzart, Surf. Coat. Technol. 107 (1998) 24.
[23] L.C. Fontana, J.R.L. Muzart, Surf. Coat. Technol. 114 (1999) 7.
[24] A.A.C. Recco, D. López, A.F. Bevilacqua, F. Silva, A.P. Tschiptschin, Surf. Coat. Technol. 202 (2007) 993.
[25] A.A.C. Recco, I.C. Oliveira, M. Massi, H.S. Maciel, A.P. Tschiptschin, Surf. Coat. Technol. 202 (2007) 1078.
[26] A.A.C. Recco, C.C. Viáfara, A. Sinatora, A.P. Tschiptschin, Wear 267 (2009) 1146.
[27] R. Ranjan, J.P. Allain, M.R. Hendricks, D.N. Ruzic, J. Vac. Sci, Technol. A 19 (3) (2001) 1004.